Improved estimates of ammonia emissions from global croplands

Xiaoying Zhan[1,2#], Wulahati Adalibieke[1#], Xiaoqing Cui[1], Wilfried Winiwarter[3,4], Stefan Reis[5,6], Lin Zhang[7], Zhaohai Bai[8], Qihui Wang[1], Weichen Huang[1], Feng Zhou[1*]

[1]College of Urban and Environmental Sciences, and Ministry of Education Laboratory for Earth Surface Processes, Peking University, Beijing 100871, PR China;

[2]Agricultural Clean Watershed Research Group, Chinese Academy of Agricultural Sciences, Institute of Environment and Sustainable Development in Agriculture, Beijing 100081, PR China;

[3]International Institute for Applied Systems Analysis (IIASA), Laxenburg A-2361, Austria;

[4]The Institute of Environmental Engineering, University of Zielona Góra, Zielona Góra 65-417, Poland;

[5]UK Centre for Ecology & Hydrology, Penicuik, EH26 0QB, United Kingdom;

[6]University of Exeter Medical School, Knowledge Spa, Truro, TR1 3HD, United Kingdom

[7]Laboratory for Climate and Ocean–Atmosphere Studies, Department of Atmospheric and Oceanic Sciences, School of Physics, Peking University, Beijing 100871, PR China;

[8]Key Laboratory of Agricultural Water Resources, Center for Agricultural Resources Research, Institute of Genetic and Developmental Biology, The Chinese Academy of Sciences, 286 Huaizhong Road, Shijiazhuang 050021, Hebei, China.

# X.Y.Z. and W.A. contributed equally to this work.

* Corresponding author: Phone / fax: +86 10 62756511; Email: zhouf@pku.edu.cn

ABSTRACT

Reducing ammonia (NH_3) volatilization from croplands while satisfying food demand is strategically required to mitigate haze pollution. However, the global pattern of NH_3 volatilization remains uncertain, primarily due to the episodic nature of NH_3 volatilization rates and the high variation of fertilization practices. Here, we improve a global estimate of crop-specific NH_3 emissions at a high spatial resolution, using an updated data-driven model with a survey-based dataset of fertilization scheme. Our estimate of globally-averaged volatilization rate (12.6% ± 2.1%) is in line with previous data-driven studies (13.3% ± 3.1%), but results in one quarter lower emissions than process-based models (16.5% ± 3.1%). The associated global emissions are estimated at 14.4 ± 2.3 Tg N, with more than 50% of the total stemming from three stable crops or 12.2% of global harvested areas. Nearly three quarters of global cropland-NH_3 emissions could be reduced by improving fertilization schemes (right rate, right type, and right placement). A small proportion (20%) of global harvested areas, primarily located in China, India, and Pakistan, accounts for 64% of abatement potentials. Our findings provide a critical reference guide for future abatement strategy design when considering locations and crop types.

INTRODUCTION

The food system, including crop and livestock production, is responsible for up to 90% of total ammonia (NH_3) volatilized from the land to the atmosphere[1-3]. Atmospheric NH_3 facilitates the formation of fine particulate matter ($PM_{2.5}$, particles with an aerodynamic diameters ≤2.5 μm) containing ammonium sulphate and nitrate compounds[4-7], which adversely impacts air quality[8] and human health[2]. Large amounts of NH_3 and its aerosol-phase products further lead to nitrogen deposition[9] and consequently to soil acidification[10], eutrophication[11-13], and changes in terrestrial carbon sinks[14] and biodiversity[15]. National policies and private sector commitments now focus on reducing NH_3 emissions from the food systems. For instance, abatement options addressing agricultural NH_3 volatilization have been adopted in the updated Clean Air Action Plan of China[10]. In European Union, NH_3 emissions are limited for each member country through National Emission Ceilings Directive[16]. Due to the growing food demand, NH_3 abatement strategies targeting fertilization schemes are not only critical to improve crop production and to reduce fertilizer waste, but also important to control $PM_{2.5}$ pollution and nitrogen depositions[17].

To assess the abatement potentials of NH_3 emissions, it is prerequisite to identify the volatilization rates (VRs) associated with diverse farming systems and fertilization practices. However, the quantification of VR (i.e., NH_3-N emission per unit of N fertilizers applied) and relevant emissions remains highly uncertain, primarily attributable to the episodic nature of NH_3 volatilization and the highly spatial variability of agricultural practices[1,2,18-21]. For example, estimates of global cropland-NH_3

volatilization from synthetic fertilizer application by various bottom-up approaches[2,18,19,21] ranged from 9 to 14 Tg N (Table S1). Such differences were as large as almost two times within the major emitting countries (e.g., China[18,22], Pakistan[19,23], USA[2,21]).

The bottom-up approach is most commonly used approach in research studies and for the compilation of NH_3 emission inventories, which is calculated as VRs multiplied by the amount of N-fertilizers applied[24,25]. Harmonized national NH_3 inventories are available for countries in Europe only and the detailed methods were published by the European Environment Agency[26]. The Intergovernmental Panel on Climate Change (IPCC), focusing to better understand indirect emissions of nitrous oxide as part of greenhouse gas (GHG) accounting, uses less extensive algorithms for NH_3 and hence assumed constant VRs (Tier 1 approach). Such constant VRs need to be complemented by detailed approaches. Bouwman et al.[27] proposed a data-driven model that simulated NH_3 volatilization incorporating the environmental and practice-related controls of VRs. This model has been gradually updated over the past two decades by refining the response of VRs to soil properties and climatic factors as well as fertilization practices[1,2,28-30]. Another type of approaches, the process-based models (e.g. FAN[18,21], DNDC[31,32], DLEM-Bi-NH_3[19]), were developed to better represent physicochemical processes of NH_3 transfer across the cropland-atmosphere interface. Both data-driven and process-based models attempt to simulate the actual emissions situation than a statistically-based Tier 1 approach are still prone to at least two types of shortcomings. Firstly, some crucial environmental factors were not adequately considered in the models, particularly for diversified farming systems and fertilization practices[1,27,28]. Secondly, systematic error associated with data-driven and process-based models are partially due to the uncertainties in the data on fertilization schemes (e.g., rate, type, timing, placement)[19,21,33]. Because high-resolution, crop- and fertilizer-specific data of N inputs are not typically available at regional or global scales from ground observations, disaggregation of national-scale data is usually performed[1,18,19,21,27,28]. Current models are therefore subject to the uncertainties not only in estimating emissions, but also in identifying global hotspots of abatement potentials.

Here, we aim to improve the global cropland-NH_3 emissions and abatement potentials in the year 2000. NH_3 emissions from the application of synthetic fertilizers, manure and crop residues returned to croplands were considered. The data-driven models were first updated by constraining the observed response of crop-specific VRs to soil and climatic attributes and fertilization practices based on globally-distributed field measurements. Its performance depends on the density and representativeness of site-level observations and the quality of gridded predictor data. We then developed global gridded maps of crop-specific fertilization schemes that were disaggregated from sub-national surveys. Our models finally provided a crop-specific, sub-national assessment on how fertilization practices interact with soil and climatic attributes to generate the global patterns of cropland-NH_3 emissions and associated abatement potentials.

MATERIALS AND METHODS

We first compiled site-based flux observations to constrain a data-driven model for NH_3 VR by crop. By combining the data-driven model and the new 5-arc-minute resolution data of fertilization schemes, we quantified the VRs and relevant emissions from 21 crop groups, but focused on the top ten crops and regions (nine individual countries plus the European Union) that contribute the most of global NH_3 emissions. We further estimated cropland-NH_3 emission intensity as total volatilization per total kilocalorie of production proposed by Carlson et al.[33], and provided insights into the tradeoffs between food security and air quality improvements. Moreover, we assessed the abatement potentials by crop and location through scenario-based simulations.

Observations. Cropland-NH_3 VRs observations were collected from 171 stations globally from peer-reviewed literatures (Figure S1). Literatures with studies back to 1970 were reviewed through Web of Science and Google Scholar. We collected data from croplands (i.e., the FAO's 'Arable land and permanent crops'), and excluded data from other land-use categories. Data from croplands (i.e., the FAO's 'Arable land and permanent crops') with the exclusion from other land-use categories were retrieved. Most of data (99%) were collected from micrometeorological techniques (mass balance methods and integrated horizontal flux method) and chamber-based (static, dynamic and wind tunnel) field studies, and only 1% from laboratory or greenhouse incubation studies (Figure S2). Moreover, data without a zero-N control or using controlled-release fertilizers or nitrification inhibitors or urease inhibitors were excluded. Final datasets include 1165 observations of cropland-NH_3 VR, twice the size of previously compiled datasets[1,28] (Data S1). VR for each non-zero N application rate (N, kg NH_3-N ha^{-1}) is defined as the difference between NH_3 volatilization at the application rate (V_N, kg NH_3-

N ha^{-1}) and control (V_0, kg NH_3-N ha^{-1}) divided by N, *i.e.*, $VR = (V_N - V_0)/N$.

For each dataset, we recorded information on five broad categories, i.e., crop-specific VR, climate (air temperature and air flow rate within the chambers), soil pH for upland crops or ponded water pH for rice paddies, fertilization scheme (rate, type, and placement), and experimental parameters (latitude, longitude, planting and harvesting dates). VR, air flow rate, fertilization, and experimental parameters were either derived based on statements in the literature sources, or supplemented by direct information obtained from authors. The remaining variables were extracted from the global data layers (CRU TS V4.03[34], HWSD v1.2[35]) based on geographic coordinates and growing seasons since they were inconsistent from various studies. Note that wind speed ($u_{0.1}$, where 0.1 m was assumed as the height of the chambers) was transferred based on the literature mentioned air flow rate using an empirical calibration equation from micrometeorological techniques[36]. It was further converted to the value at the height of 10 m (u_{10}) based on a power law calculation (i.e. $u_{10} = u_{0.1} \times (10/0.1)^{\alpha}$, where α was set as 0.1 and 0.15 for rice paddies and upland due to the different surface roughness[37], respectively.

Model. We estimated NH_3 VRs separately for upland crops and rice paddies as a function of meteorological conditions, soil properties, and fertilization scheme. This type of function has been widely applied in previous bottom-up estimates[29,30,38] as follows:

$$VR_{i,k} = VR_i^0 \times f(pH_{i,k}) \times f(A_{i,k}) \times f(u_{i,k}) \times f(T_{i,k}) \times f(M_{i,k}), \tag{1a}$$

$$V_{i.k} = VR_{i,k} \times N_{i,k} \times H_{i,k} \tag{1b}$$

where $VR_{i,k}$ is NH_3 volatilization rate for crop i in grid k. i=1 to 21, corresponding to different crops (Table S2). V, N, and H represent NH_3 volatilization, total N application rate and harvested area, respectively. VR^0 is averaged from available VR data, roughly corresponding to the baseline of VR under reference condition (i.e., chamber-based using urea applied through broadcasting with soil pH of 7 and air temperature of 20°C for upland crops or of 26°C for paddy rice, Data S1 and Table S3). $f(pH)$, $f(A)$, $f(u)$, $f(T)$, and $f(M)$ represent the correction coefficients that reflect the effects of pH, air temperature and wind speed (u_{10}) during the period of crop growth, fertilizer type, and placement on VR, respectively. The form of $f(pH)$ and $f(A)$ was determined as an exponential function because pH governs the NH_4^+-aqueous NH_3 equilibrium and temperature modulates the reaction velocities related to both equilibrium and transfer across the water-air interface[39]. The form of $f(u)$ was determined as a logarithmic function due to the existence of a threshold of NH_3 volatilization induced by wind[31,40-42]. The form of $f(T)$ and $f(M)$ were determined based on the observations from manipulation experiments using the ordinary least-square method, which were in general consistent with previous meta-analysis[43,44] (Table S4). More details on the quantification of VR^0 and correction coefficients were provided in Text S1, Table S5 and Figure S3.

Mapping. The global patterns of crop-specific NH_3 VRs and associated emissions for the year 2000 were simulated using the updated data-driven models and global gridded datasets at 5 arc-minute spatial resolution. A Monte Carlo simulation was used to estimate the overall uncertainty of cropland-NH_3 volatilization by varying all of the input data and parameters (Text S2). Crop-specific harvested areas at 5-arc-minute resolution in 2000 were obtained directly from the EARTHSTAT dataset[45]. Mean daily air temperature and wind speed (at 10 m) over the growing season were acquired from the CRU TS V4.03[34] climate dataset (0.5°×0.5°) and TerraClimate dataset (2.5′×2.5′)[46], respectively, where the growing season in each grid cell was identified as the period between the planting and harvesting dates obtained from Sacks et al[47]. For crops without a gridded crop calendar, we assumed that they grew throughout the whole year. Soil pH (pH_s) were extracted from the Harmonized World Soil Database (HWSD) v1.2 (1×1 km)[35]. This data can be used directly for upland crops, but has to be converted into pH in ponded water (pH_w) for paddy rice. Based on previous observations[48], we modeled pH_w as a function of pH_s and N application rate, i.e., $pH_w = 0.0012^{+0.0002}_{-0.0002} \times N + pH_s + 0.2056^{+0.0345}_{-0.0345}$ (R^2=0.51, n=25, p<0.01; Figure S4). Both climate and soil properties were re-gridded to a resolution of 5′ × 5′ using a first-order conservative interpolation method[49].

A global gridded crop-specific fertilization scheme dataset for the year 2000 was specifically developed for this study, including the rate, type, and placement of N inputs. First, we acquired the total N application for 15,790 global administrative units[50], mainly based on the sub-national statistics of synthetic fertilizer application rates obtained from local statistical agencies in 38 countries. Gridded data of manure applications from Zhang et al.[51], and the country-level statistics of crop residues applied to croplands were taken from FAOSTAT[52]. It should be noted that all fertilizer inputs represent the amount applied only to croplands, livestock housing and manure storage are excluded. Second, to calculate the crop-specific N application rates, we allocated total N inputs for 21 specific crops for each administrative unit based on the previously-developed proportions of total fertilizer use by crop from the EARTHSTAT dataset (5′×5′)[45]. Third, we further allocated the proportion of 11 types of synthetic fertilizers for all crops based on the 113 provincial or state-level statistics for China[53], USA[54], and India[55] and the IFA's national statistics for all other countries[56] (Figure S5). N application rates by crop and fertilizer were then disaggregated into grid maps at 5-arc-minute spatial resolution following the EARTHSTAT's harvested area distributions within each of the administrative units. To exclude unrealistic values, the maximum combined synthetic + manure + crop residues N-application rate was set to be 1,000 kg N ha^{-1} based on results from previous studies[50].

Last, we determined the fraction of different placement methods in each grid cell according to fertilizer type and tillage practice. Anhydrous ammonia and N solutions, which are commonly injected, are deeply placed and totally incorporated into soils, respectively, whereas for other synthetic fertilizer application we simply assumed that the broadcasting techniques were applied[28]. Manure and crop residues are usually applied before sowing or transplanting and afterwards are incorporated linearly in response to tillage fraction[1,57]. Data of no-tillage fraction by crop and province (or state) were publicly available for China (2000-2008)[58] and the USA (1989-2008)[59]. Country-level no-tillage fractions were further obtained for another 46 countries from the FAOSTAT[52] and EUROSTAT databases[60]. For other countries, the no-tillage fraction (η_i) was estimated by the predictive equation calibrated by abovementioned data, i.e.,

$\eta_i = 0.0190^{+0.0024}_{-0.0024} y_n^{\,2} - 0.0226^{+0.0110}_{-0.0110} y_n + 0.0331^{+0.0102}_{-0.0102}$ (n = 70, R^2 = 0.802, $p <$ 0.001), where y_n is the cropland area per capita of rural population[52,61] in country n that represents the spatial variation of labor availability for tillage activity (Figure S6). All the crops share the same no-tillage proportion at country-level for counties except China and the USA.

Abatement potential assessment. We developed three scenarios to identify the global hotspots of NH_3 abatement potentials. The three scenarios aimed to assess the effectiveness of improved fertilization schemes (e.g. right quantity, type, and placement): (i) scenario 1 where total N input were reduced to achieve the crop-specific N use efficiency (NUE) targets determined by Zhang et al.[62] without decrease in crop yields (S1); (ii) scenario 2 where the proportion of two alkaline fertilizers (i.e., ABC and urea) was capped at the same level as that in the USA in 2000 (i.e., 21.8% of total synthetic fertilizers)[54] and all fertilizers except anhydrous ammonia were incorporated in soils (S2); (iii) S1+S2 representing the combination of scenarios 1 and 2. Note that our objective was to assess the abatement potentials, rather than to optimize the measures considering technical or socio-economic barriers. For scenario 1, we first estimated the global cropland N surplus (N_{sur}) by grid and crop as the sum of N inputs (fertilizers, manure, biological fixation, and atmospheric depositions) minus N outputs (N_{yield}). Biologically fixed N and N_{yield} were calculated based on the crop yield data from EUROSTAT databases (0.5′×0.5′) and the parameters (nitrogen fixation rate and N content by crop) from previous studies[62]. Atmospheric depositions of N were extracted from the IGAC/SPARC Chemistry-Climate Model Initiative[63] (0.5°×0.5°)

over global croplands. Second, we estimated the reduction in N surplus (ΔN_{sur}) by increasing NUE to be the crop-specific targets (NUE_{tar}), i.e., $\Delta N_{sur} = N_{sur} - N_{yield} \cdot (1/NUE_{tar} - 1)$. We finally used the data-driven model to quantify the NH_3 emissions by crop using the reduced N application rate where applicable, i.e., $N - \Delta N_{sur}$, and thereby the NH_3 VR as well as abatement potentials by crop.

RESULTS

Emissions. In 2000, globally averaged cropland-NH_3 VR was estimated as 12.6 ± 2.1% (mean ± standard deviation, Figure 1). Our estimates of VRs were within the range of previous results of data-driven models at both global (9.7% ~17.0%) and regional scales (Figure 1). This is also aligned the Tier 1 default of 2019 refinement to IPCC guidelines (12.1%, VR weighted by fertilizer types, Data S1)[24]. However, the VRs estimated by our new model were ~24% lower than the mean values of process-based models at a global scale. Similar discrepancies were mainly found in the USA and EU, but not in China, India or Pakistan where the estimates were highest in the world (Figure 1). In addition, cotton and rice had the largest VRs (23.7% ± 1.9% and 15.1% ± 7.7%, respectively, Figure 2a), followed by sugar crops (13.4% ± 1.2%), wheat (13.3% ± 1.0%), and maize (12.7% ± 1.1%). The smallest VRs were found for oil crops (10.5% ± 0.9%) and other cereals (9.1% ± 2.1%).

<<Figure 1>>

Our estimate also suggests that NH_3 VRs were significantly different from one region to another (Figure 2a), yet the patterns were generally similar among major crops (Figure S7). VRs from Pakistan, Iraq, India, and the North China Plain were twice as large as the global average, largely due to the favorable environmental conditions for NH_3 volatilization with more alkaline soils and higher air temperature during growing seasons. In contrast, VRs from South America, Southeast Asia, and Oceania were about 50% below the global average since the soil pH is quite low (~5.5) in these regions. In other regions like the USA and EU, VRs were relatively small (~6.4% and ~5.0%) mainly due to the wide use of liquid fertilizers (e.g., N solutions and anhydrous ammonia) and acid fertilizers (e.g., ammonium nitrate, calcium ammonium nitrate, and ammonium sulfate), plus the prevalence of acidic soils in these regions (Figure S5).

<<Figure 2>>

Our estimate suggests that the global cropland-NH_3 emissions (14.4 ± 2.3 Tg N) represented nearly one third (31%) of the total global anthropogenic NH_3 emissions in 2000[25]. This quantity was equivalent to 13-18% of crop N uptake (including grass) and 25%-31% of the N losses through leaching and runoff estimated by previous studies[64,65] (Table S6). The top ten emitting crops accounted for 93% of global emissions, in which 21% of the total were from paddy rice, 21% from wheat, 15% from maize, and 12% from vegetables and fruits (Figure 2b). The spatial distribution of cropland-NH_3 volatilization by crop was similar to those of VRs (Figure S7 and S8), but emission hotspots were amplified in high-N-rate regions (>150 kg N ha^{-1}). More than 50% of the global NH_3 emissions were from 12.2% of the croplands (Figure S9). The highest emission regions were concentrated in China, India, Pakistan the USA and EU, contributing 71% of global emissions (see details in Table S7).

Emission intensities. We further defined the global mean emission intensity[33] as the cropland-NH_3 volatilization divided by total kilocalorie production. The latter was quantified based on the gridded crop production from the EARTHSTAT database[45] and the calorie conversion factors by crop and country[33]. Global mean emission intensity was estimated as 1.28 ± 0.21 mg NH_3-N kcal^{-1}. Regions with the highest intensity were Pakistan, India, Iraq, the North China Plain, and those near the border between the United States and Mexico (Figure 2c). We further found that cropping practices contributed disproportionately to NH_3 volatilization and crop kilocalories (Figure 3a). In general, crops used for food (e.g., rice, wheat) tend to have high emission intensities, whereas crops mainly for non-food uses (e.g., maize, soybean, barley) are associated with lower emission intensities. For example, rice (1.8 ± 0.93 mg NH_3-N kcal^{-1}), which is highly concentrated in Asia accounted for 21% of these cropland emissions, while suppling only 15% of total crop kilocalories. Maize, producing 19% of total crop kilocalories, generated only 15% of cropland emissions.

Emission intensity was also dependent on locations (Figure 3b). For example, Pakistan was the third largest emitter, while having the highest emission intensity (6.91 ± 0.54 mg NH_3-N kcal^{-1}). In contrast, the USA and EU supplied one third of total crop kilocalories, but contributed less than 11% of cropland-NH_3 emissions. Emissions intensities were at $0.39 \sim 1.59$ mg NH_3-N kcal^{-1} in developed countries, but were substantially larger in developing countries (1.17 ~ 6.91 mg NH_3-N $kcal^{-1}$). We also find considerable subnational heterogeneity of NH_3 emission intensities by crop (Figure S10).

<<Figure 3>>

Abatement potentials. Reductions in N inputs and VRs are two approaches to mitigate cropland-NH_3 emissions. When achieving the crop-specific NUE targets determined by Zhang et al.[62] (S1), global cropland-NH_3 emissions would be reduced by 7.5 Tg N, accounting for 52.1% of the total (14.4 Tg N) in the year 2000 (Table S8). When conducting fertilizer type adjustment and universal use of deep placement together (S2), global cropland-NH_3 emissions would be reduced by 7.1 Tg N (or 49.4% of the total) (Table S8). When combining the measures from both scenarios (S1+S2), the abatement potentials would increase to 10.8 Tg N, contributing to 75.1% of the global cropland-NH_3 emissions (Table S8). Based on our spatially-explicit estimates, a small proportion (20%) of global harvested areas accounts for ~63% of global abatement potentials regardless of scenarios (Figure 4a, b, and c). Such 20% of global harvested areas contribute more proportion of abatement potentials for wheat (66-70%) and vegetables and fruits (63-66%), but less for the other crops (<54%). In other words, large NH_3 reductions could be achieved in a small part of croplands, depending on the gap between current and targeted fertilization schemes (i.e., rate, type, and placement), crop mix, and local environmental conditions.

<<Figure 4>>

For S1, most of abatement potentials (7.5 Tg N) were concentrated in Asia where the NUE needs to be substantially improved (Figure 5a), with 32% of the potential in China (2.4 Tg N), 26% in India (2.0 Tg N), and 8% in Pakistan (0.6 Tg N). Parts of the croplands in Mongolia, South America and Sub-Saharan Africa may need to reduce NH_3 emissions by more than half to meet their crop-specific NUE targets (Figure 5b). The abatement potentials in China increased up to 2.7 Tg N for S2, accounting for 38.7% of the total potentials (7.1 Tg N), while for Pakistan and India, the potential decreased down to 0.37 and 1.5 Tg N, respectively (Figure 5c). Such discrepancies were attributed to larger applications of alkaline fertilizers and surface broadcasting in China, implying that more than a half of NH_3 emissions should be reduced primarily in this country (Figure 5d). Despite no significant differences in the spatial patterns of abatement potentials between three scenarios (Figures 5a, c, and e), more than 70% of global harvested areas had the abatement potentials to that are over 50% of their NH_3 emissions (Figure 5f).

<<Figure 5>>

DISCUSSION

In this study, we demonstrated the potentials of using data-driven VRs and survey-based gridded fertilization schemes to accurately estimate global cropland-NH_3

emissions. Large discrepancies between our estimates and previous studies may arise from the differences related to model parameterization and input datasets. First, the sensitivities of NH_3 fluxes to environmental or management-related variables, either for empirical or process-based approaches, were typically validated by limited observations or manipulation experiments[18,19,21]. In our study, about 1,000 measurements were collected representing a wide range of environmental and management-related conditions to quantify the baseline and correction coefficients of VRs. Second, global dataset of N fertilization schemes have not been accurately quantified in most of previous studies[1,18,19,21,27,28]. For instance, fertilizer types were either ignored[19] or simply took urea as the default fertilizer for N inputs[21]. Although urea has been widely applied in Asia, it does not in Europe, Sub-Saharan Africa or Brazil where acid fertilizers, manure, and crop residues accounted for more than 50% of total N inputs (Figure S5), which might explain the reason why the FAN v1 model (9%)[21] overestimated European NH_3 volatilization rates by 80% compared to our results (5%; Figure S11). Fertilizer placement is another key factor influencing the convective and diffusive transport of fertilizers in the soil[39], which was often assumed as a universal broadcasting technique for synthetic fertilizers or as an incorporation for manure returned to croplands[19,21,28]. However, fertilizer broadcasting placement is only popular in Asia, but not in the USA, where ~50% of synthetic fertilizers (anhydrous ammonia and N solutions) are injected into soils (Figure S5). Taking into consideration of the difference in broadcasting method in the USA, our estimates of the cropland-NH_3 VR in USA was greatly decreased, i.e., 6% [our estimate] compared to 16% [FAN v1[21]] in previous studies, Figure S11). Third, soil or ponded water pH have not been adequately simulated in some previous studies[19,21]. For instance, pH values were fixed as a constant value (e.g., 7[21] or 7.5[19]) within a week after fertilization. This assumption might not be applicable in the North China Plain, India, and Pakistan since the background soil pH is above 7.5 there. To validate our theory, additional sensitivity tests (assuming pH = 7) were performed and the test results well explained the underestimations by the FAN v1[21] and DLEM-Bi-NH_3[19] models for the aforementioned three countries (Text S3 and Figure S11).

Further work needs to be done to determine the reliability of our estimates compared to the state-of-the-art emission inventories. First, our estimate of VR is subject to uncertainties due to not accounting for the effects of soil moisture due to precipitation and irrigation[66]. Increasing soil moisture would stimulate the rate of hydrolysis and thereby NH_3 volatilization[39]. However, excessive water inputs may, in turn, constrain NH_3 volatilization by eluting fertilizers into the deep soil allowing NH_4^+ to be adsorbed[44]. Second, our models do not consider the effect of splitting N fertilizer application. One-time fertilizer application was assumed in this study, which might not be the case in China, Europe or USA[19]. Third, we assumed that synthetic fertilizers, except anhydrous ammonia and N solutions, were applied through surface broadcasting following previous studies[1,27,28]. While surface broadcasting is common in China, it might not be in developed countries[54,67]. Last but not the least, we did not differentiate the liquid manure application (usually injected into soil) from the solid manure systems, which may lead to the overestimation of VR. Similarly, we assumed that the VR of crop residues was comparable to those of manure. Such assumption may result in the overestimation of NH_3 emissions, as crop residues carry less inorganic N and slower mineralization rate of organic N[39].

Despite the aforementioned uncertainties, our assessment provided consistent metrics that are relevant across scales and useful for identifying the global hotspots of NH_3 emissions. Such flexibility is valuable for making decisions when abatement measures must be taken for specific regions. Reducing excess N application could not only mitigate NH_3 volatilization substantially, but also the other reactive N losses to achieve the targeted NUE. The effective implementation of such measure depends on how reasonable the technical or socio-economic barriers are addressed. Fertilizer type adjustment and deep placement, despite a smaller abatement potentials and a less economic benefits, may be easily accepted to implement in the short term when providing subsidies to the farmers[68]. The choice of different measures also depends on crop-specific yield response as well as fertilization-related technical support, local policy interventions, and farmers' perception[69]. In addition, our assessment highlights that total NH_3 volatilization is largely unrelated to crop productions, suggesting the potential conflict between air quality and food security goals (Figure 3). Shift in crop mix based on their emissions intensities could further reduce the overall emission intensity of croplands. Changing patterns of crop mixes could be realized through international and national food trades, considering local climate and edaphic conditions, dietary diversity and the nutritional value of food provision. Targeting abatement efforts at locations with both high intensities and high emissions is therefore likely to be a more effective strategy than focusing solely on large emitters.

Food demand is projected to increase substantially by 2050[33]. The solutions to satisfy the increasing food demand while reducing reactive N losses will require cross-disciplinary collaborations, such as: (1) developing innovative technology and management systems for fertilization, irrigation, and tillage to be economically viable and readily adopted by farmers[62]; (2) conducting field-scale comparative experiments to identify the measures to avoid pollution swapping (a measure designed to address NH_3 emission leads to other reactive N losses; for example, fertilizer incorporation can reduce NH_3 emissions, but may lead to high nitrate leaching especially for wet climates[65]); (3) designing large-scale action plan to advance science-based nutrient management such as the application of slow-release N fertilizers, promotion of crop rotation, and sowing of cultivar mixtures[70].

In conclusion, our spatially-explicit cropland-NH_3 emission data could be used to support and guide the development of such interventions, which may include farmer education through extension and outreach, scientist-farmer collaboration, national food policies, and national and international food trade. Moreover, it is critical to apply regionally-specific approaches to refine NH_3 volatilization models and mitigate measures to specific subnational regions. Producers need supports to better manage N fertilization practice for increasing NUE, and to implement region-specific techniques to avoid favorable environmental conditions for all reactive N losses. Future research evaluating the tradeoffs among NH_3 volatilizations, other reactive N release and food security should consider both food production and the nutritional value of the food production, which is promising to reduce the NH_3 emission intensity from croplands globally.

SUPPORTING INFORMATION

Extended explanation of cropland-NH_3 VR model, model inputs, uncertainty estimates, comparison with previous estimates, cropland NH_3 VRs observations, and associated supplementary Tables and Figures are all available free of charge at http://pubs.acs.org.

AUTHOR INFORMATION

Corresponding Author

* Phone: +86 10 62756511, Fax: +86 10 62756560; Email: zhouf@pku.edu.cn.

Notes

The authors declare no competing financial interest.

ACKNOWLEDGMENT

This study was supported by the National Natural Science Foundation of China (71961137011; 41907087), the National Key Research and Development Program of China (2018YFC0213304), Central Public-interest Scientific Institution Basal Research Fund (BSRF201905) and the Youth Fund of Ministry of Education Laboratory for Earth Surface Processes, Peking University. This publication also contributes to UNCNET, a project funded under the JPI Urban Europe / China collaboration with project numbers UMO-2018/29 / Z / ST10 / 0298 (NCN, Poland) and 870234 (FFG, Austria). The contribution by S.R. was supported by the UK Natural

Environment Research Council (NERC) National Capability award NE/R000131/1, SUNRISE Sustainable Use of Natural Resources, Improve human health and Support Economic development working in partnership with researchers and agencies internationally (https://www.ceh.ac.uk/our-science/projects/sunrise).

REFERENCES

1. Beusen, A. H. W.; Bouwman, A. F.; Heuberger, P. S. C.; Van Drecht, G.; Van Der Hoek, K. W. Bottom-up uncertainty estimates of global ammonia emissions from global agricultural production systems. *Atmos. Environ.* **2008,** *42* (24), 6067-6077.

2. Paulot, F.; Jacob, D. J.; Pinder, R. W.; Bash, J. O.; Travis, K.; Henze, D. K. Ammonia emissions in the United States, European Union, and China derived by high-resolution inversion of ammonium wet deposition data: Interpretation with a new agricultural emissions inventory (MASAGE_NH_3). *J. Geophys. Res.-Atmos.* **2014,** *119* (7), 4343-4364.

3. Emissions Database for Global Atmospheric Research V4.3.2. https://edgar.jrc.ec.europa.eu/overview.php?v=432_AP.

4. Lelieveld, J.; Evans, J. S.; Fnais, M.; Giannadaki, D.; Pozzer, A. The contribution of outdoor air pollution sources to premature mortality on a global scale. *Nature* **2015,** *525* (7569), 367-371.

5. Tang, Y. S.; Braban, C. F.; Dragosits, U.; Dore, A. J.; Simmons, I.; van Dijk, N.; Poskitt, J.; Pereira, G. D.; Keenan, P. O.; Conolly, C.; Vincent, K.; Smith, R. I.; Heal, M. R.; Sutton, M. A. Drivers for spatial, temporal and long-term trends in atmospheric

ammonia and ammonium in the UK. *Atmos. Chem. Phys.* **2018,** *18* (2), 705-733.

6. Kong, L.; Tang, X.; Zhu, J.; Wang, Z. F.; Pan, Y. P.; Wu, H. J.; Wu, L.; Wu, Q. Z.; He, Y. X.; Tian, S. L.; Xie, Y. Z.; Liu, Z. R.; Sui, W. X.; Han, L. N.; Carmichael, G. Improved Inversion of Monthly Ammonia Emissions in China Based on the Chinese Ammonia Monitoring Network and Ensemble Kalman Filter. *Environ. Sci. Technol.* **2019,** *53* (21), 12529-12538.

7. Wang, M. Y.; Kong, W. M.; Marten, R.; He, X. C.; Chen, D. X.; Pfeifer, J.; Heitto, A.; Kontkanen, J.; Dada, L.; Kürten, A.; Yli-Juuti, T.; Manninen, H. E.; Amanatidis, S.; Amorim, A.; Baalbaki, R.; Baccarini, A.; Bell, D. M.; Bertozzi, B.; Bräkling, S.; Brilke, S.; Murillo, L. C.; Chiu, R.; Chu, B. W.; Menezes, L. D.; Duplissy, J.; Finkenzeller, H.; Carracedo, L. G.; Granzin, M.; Guida, R.; Hansel, A.; Hofbauer, V.; Krechmer, J.; Lehtipalo, K.; Lamkaddam, H.; Lampimäki, M.; Lee, C. P.; Makhmutov, V.; Marie, G.; Mathot, S.; Mauldin, R.; Mentler, B.; Müller, T.; Onnela, A.; Partoll, E.; Petäjä, T.; Philippov, M.; Pospisilova, V.; Ranjithkumar, A.; Rissanen, M.; Rörup, B.; Scholz, W.; Shen, J. L.; Simon, M.; Sipilä, M.; Steiner, G.; Stolzenburg, D.; Tham, Y. J.; Tomé, A.; Wagner, A. C.; Wang, D. Y. S.; Wang, Y. H.; Weber, S. K.; Winkler, P. M.; Wlasits, P. J.; Wu, Y. S.; Xiao, M.; Ye, Q.; Zauner-Wieczorek, M.; Zhou, X. Q.; R., V.; RiipinenI, l.; Dommen, J.; Curtius, J.; Baltensperger, U.; Kulmala, M.; Worsnop, D. R.; Kirkby, J.; Seinfeld, J. H.; El-Haddad, I.; Flagan, R. C.; Donahue, N. M. Rapid growth of new atmospheric particles by nitric acid and ammonia condensation. *Nature* **2020,** *581*, 184–189.

8. Huang, R. J.; Zhang, Y. L.; Bozzetti, C.; Ho, K. F.; Cao, J. J.; Han, Y.; Daellenbach,

K. R.; Slowik, J. G.; Platt, S. M.; Canonaco, F.; Zotter, P.; Wolf, R.; Pieber, S. M.; Bruns, E. A.; Crippa, M.; Ciarelli, G.; Piazzalunga, A.; Schwikowski, M.; Abbaszade, G.; Schnelle-Kreis, J.; Zimmermann, R.; An, Z.; Szidat, S.; Baltensperger, U.; Haddad, I. E.; Prévôt, A. S. H. High secondary aerosol contribution to particulate pollution during haze events in China. *Nature* **2014,** *514*, 218–222.

9. Li, Y.; Schichtel, B. A.; Walker, J. T.; Schwede, D. B.; Chen, X.; Lehmann, C. M. B.; Puchalski, M. A.; Gay, D. A.; Collett, J. L. Increasing importance of deposition of reduced nitrogen in the United States. *Proc. Natl. Acad. Sci. U. S. A.* **2016,** *113* (21), 5874-5879.

10. Liu, M. X.; Huang, X.; Song, Y.; Tang, J.; Cao, J. J.; Zhang, X. Y.; Zhang, Q.; Wang, S. X.; Xu, T. T.; Kang, L.; Cai, X. H.; Zhang, H. S.; Yang, F. M.; Wang, H. B.; Yu, J. Z.; Lau, A. K. H.; He, L. Y.; Huang, X. F.; Duan, L.; Ding, A. J.; Xue, L. K.; Gao, J.; Liu, B.; Zhu, T. Ammonia emission control in China would mitigate haze pollution and nitrogen deposition, but worsen acid rain. *Proc. Natl. Acad. Sci. U. S. A.* **2019,** *116* (16), 7760-7765.

11. Elser, J. J.; Andersen, T.; Baron, J. S.; Bergstrom, A. K.; Jansson, M.; Kyle, M.; Nydick, K. R.; Steger, L.; Hessen, D. O. Shifts in Lake N:P Stoichiometry and Nutrient Limitation Driven by Atmospheric Nitrogen Deposition. *Science* **2009,** *326* (5954), 835-837.

12. Wang, R.; Balkanski, Y.; Bopp, L.; Aumont, O.; Boucher, O.; Ciais, P.; Gehlen, M.; Penuelas, J.; Ethe, C.; Hauglustaine, D.; Li, B. G.; Liu, J. F.; Zhou, F.; Tao, S. Influence of anthropogenic aerosol deposition on the relationship between oceanic

productivity and warming. *Geophys. Res. Lett.* **2015,** *42* (24), 10745-10754.

13. Zhan, X. Y.; Bo, Y.; Zhou, F.; Liu, X. J.; Paerl, H. W.; Shen, J. L.; Wang, R.; Li, F. R.; Tao, S.; Dong, Y. J.; Tang, X. Y. Evidence for the Importance of Atmospheric Nitrogen Deposition to Eutrophic Lake Dianchi, China. *Environ. Sci. Technol.* **2017,** *51* (12), 6699-6708.

14. Wang, R.; Goll, D.; Balkanski, Y.; Hauglustaine, D.; Boucher, O.; Ciais, P.; Janssens, I.; Penuelas, J.; Guenet, B.; Sardans, J.; Bopp, L.; Vuichard, N.; Zhou, F.; Li, B. G.; Piao, S. L.; Peng, S. S.; Huang, Y.; Tao, S. Global forest carbon uptake due to nitrogen and phosphorus deposition from 1850 to 2100. *Glob. Change Biol.* **2017,** *23* (11), 4854-4872.

15. Sutton, M. A.; Mason, K. E.; Sheppard, L. J.; Sverdrup, H.; Haeuber, R.; Hicks, W. K., *Nitrogen Deposition, Critical Loads and Biodiversity*. Springer Netherlands: 2014.

16. European Environment Agency. https://www.eea.europa.eu/data-and-maps/indicators/eea-32-ammonia-nh3-emissions-1.

17. Tan, J. N.; Fu, J. S.; Seinfeld, J. H. Ammonia emission abatement does not fully control reduced forms of nitrogen deposition. *Proc. Natl. Acad. Sci. U. S. A.* **2020,** *117* (18), 9771-9775.

18. Vira, J.; Hess, P.; Melkonian, J.; Wieder, W. R. An improved mechanistic model for ammonia volatilization in earth system models: flow of agricultural nitrogen, version 2 (FAN v2). *Geoscientific Model Development Discussions* **2019**, 1-49.

19. Xu, R. T.; Tian, H. Q.; Pan, S. F.; Prior, S. A.; Feng, Y. C.; Batchelor, W. D.; Chen,

J.; Yang, J. Global ammonia emissions from synthetic nitrogen fertilizer applications in agricultural systems: Empirical and process-based estimates and uncertainty. *Glob. Change Biol.* **2019,** *25* (1), 314-326.

20. Zhan, X. Y.; Chen, C.; Wang, Q. H.; Zhou, F.; Hayashi, K.; Ju, X. T.; Lam, S. K.; Wang, Y. H.; Wu, Y. L.; Fu, J.; Zhang, L. P.; Gao, S. S.; Hou, X. K.; Bo, Y.; Zhang, D.; Liu, K. W.; Wu, Q. X.; Su, R. R.; Zhu, J. Q.; Yang, C. L.; Dai, C. M.; Liu, H. B. Improved Jayaweera-Mikkelsen model to quantify ammonia volatilization from rice paddy fields in China. *Environ. Sci. Pollut. Res.* **2019,** *26* (8), 8136-8147.

21. Riddick, S.; Ward, D.; Hess, P.; Mahowald, N.; Massad, R.; Holland, E. Estimate of changes in agricultural terrestrial nitrogen pathways and ammonia emissions from 1850 to present in the Community Earth System Model. *Biogeosciences* **2016,** *13* (11), 3397-3426.

22. Zhang, X. M.; Wu, Y. Y.; Liu, X. J.; Reis, S.; Jin, J. X.; Dragosits, U.; Van Damme, M.; Clarisse, L.; Whitburn, S.; Coheur, P. F.; Gu, B. J. Ammonia Emissions May Be Substantially Underestimated in China. *Environ. Sci. Technol.* **2017,** *51* (21), 12089-12096.

23. Yan, X. Y.; Akimoto, H.; Ohara, T. Estimation of nitrous oxide, nitric oxide and ammonia emissions from croplands in East, Southeast and South Asia. *Glob. Change Biol.* **2003,** *9* (7), 1080-1096.

24. Calvo Buendia, E.; Tanabe, K.; Kranjc, A.; Baasansuren, J.; Fukuda, M.; Ngarize, S.; Osako, A.; Pyrozhenko, Y.; Shermanau, P.; Federici, S. *2019 Refinement to the 2006 IPCC Guidelines for National Greenhouse Gas Inventories*; Switzerland, 2019.

25. Crippa, M.; Solazzo, E.; Huang, G. L.; Guizzardi, D.; Koffi, E.; Muntean, M.; Schieberle, C.; Friedrich, R.; Janssens-Maenhout, G. High resolution temporal profiles in the Emissions Database for Global Atmospheric Research. *Sci. Data* **2020,** *7* (1), 1-17.

26. EMEP/EEA air pollutant emission inventory guidebook 2019. Technical guidance to prepare national emission inventories. EEA Report No 13/2019, European environment Agency, Copenhagen. doi:10.2800/293657.

27. Bouwman, A. F.; Lee, D. S.; Asman, W. A. H.; Dentener, F. J.; VanderHoek, K. W.; Olivier, J. G. J. A global high-resolution emission inventory for ammonia. *Glob. Biogeochem. Cycle* **1997,** *11* (4), 561-587.

28. Bouwman, A. F.; Boumans, L. J. M.; Batjes, N. H. Estimation of global NH_3 volatilization loss from synthetic fertilizers and animal manure applied to arable lands and grasslands. *Glob. Biogeochem. Cycle* **2002,** *16* (2), 16.

29. Huang, X.; Song, Y.; Li, M. M.; Li, J. F.; Huo, Q.; Cai, X. H.; Zhu, T.; Hu, M.; Zhang, H. S. A high-resolution ammonia emission inventory in China. *Glob. Biogeochem. Cycle* **2012,** *26*, 1-14.

30. Zhang, Y. S.; Luan, S. J.; Chen, L. L.; Shao, M. Estimating the volatilization of ammonia from synthetic nitrogenous fertilizers used in China. *J. Environ. Manage.* **2011,** *92* (3), 480-493.

31. Dubache, G.; Li, S. Q.; Zheng, X. H.; Zhang, W.; Deng, J. Modeling ammonia volatilization following urea application to winter cereal fields in the United Kingdom by a revised biogeochemical model. *Sci. Total Environ.* **2019,** *660*, 1403-1418.

32. Li, S. Q.; Zheng, X. H.; Zhang, W.; Han, S. H.; Deng, J.; Wang, K.; Wang, R.; Yao, Z. S.; Liu, C. Y. Modeling ammonia volatilization following the application of synthetic fertilizers to cultivated uplands with calcareous soils using an improved DNDC biogeochemistry model. *Sci. Total Environ.* **2019,** *660*, 931-946.

33. Carlson, K. M.; Gerber, J. S.; Mueller, N. D.; Herrero, M.; MacDonald, G. K.; Brauman, K. A.; Havlik, P.; O'Connell, C. S.; Johnson, J. A.; Saatchi, S.; West, P. C. Greenhouse gas emissions intensity of global croplands. *Nat. Clim. Chang.* **2017,** *7* (1), 63-68.

34. CRU TS V4.30. https://crudata.uea.ac.uk/cru/data/hrg/.

35. FAO/IIASA/ISRIC/ISS-CAS/JRC. Harmonized World Soil Database V1.2. http://www.fao.org/soils-portal/soil-survey/soil-maps-and-databases/harmonized-world-soil-database-v12/en/.

36. Pacholski, A.; Cai, G. X.; Nieder, R.; Richter, J.; Fan, X. H.; Zhu, Z. L.; Roelcke, M. Calibration of a simple method for determining ammonia volatilization in the field - comparative measurements in Henan Province, China. *Nutr. Cycl. Agroecosyst.* **2006,** *74* (3), 259-273.

37. Gualtieri, G.; Secci, S. Comparing methods to calculate atmospheric stability-dependent wind speed profiles: A case study on coastal location. *Renew. Energy* **2011,** *36* (8), 2189-2204.

38. Misselbrook, T. H.; Sutton, M. A.; Scholefield, D. A simple process-based model for estimating ammonia emissions from agricultural land after fertilizer applications. *Soil Use Manage.* **2004,** *20* (4), 365-372.

39. Sommer, S. G.; Schjoerring, J. K.; Denmead, O. T., Ammonia emission from mineral fertilizers and fertilized crops. In *Advances in Agronomy*, Sparks, D. L., Ed. Elsevier Academic Press Inc.: San Diego, 2004; Vol. 82, pp 557-622.

40. Kang, Y. N.; Liu, M. X.; Song, Y.; Huang, X.; Yao, H.; Cai, X. H.; Zhang, H. S.; Kang, L.; Liu, X. J.; Yan, X. Y.; He, H.; Zhang, Q.; Shao, M.; Zhu, T. High-resolution ammonia emissions inventories in China from 1980 to 2012. *Atmos. Chem. Phys.* **2016,** *16* (4), 2043-2058.

41. Kissel, D. E.; Brewer, H. L.; Arkin, G. F. Design and test of a field sampler for ammonia volatilization. *Soil Science Society of America Journal* **1977,** *41* (6), 1133-1138.

42. Zou, C. M.; Yan, X. Y.; Yagi, K. Measurements of Ammonia Volatilization from Paddy Soils. *Chinese Agricultural Science Bulletin* **2005,** *21* (2), 167-170 (in Chinese with English Abstract).

43. Pan, B. B.; Lam, S. K.; Mosier, A.; Luo, Y. Q.; Chen, D. L. Ammonia volatilization from synthetic fertilizers and its mitigation strategies: A global synthesis. *Agric. Ecosyst. Environ.* **2016,** *232*, 283-289.

44. Ti, C. P.; Xia, L. L.; Chang, S. X.; Yan, X. Y. Potential for mitigating global agricultural ammonia emission: A meta-analysis. *Environ. Pollut.* **2019,** *245*, 141-148.

45. Monfreda, C.; Ramankutty, N.; Foley, J. A. Farming the planet: 2. Geographic distribution of crop areas, yields, physiological types, and net primary production in the year 2000. *Glob. Biogeochem. Cycle* **2008,** *22* (1), 1-19.

46. Abatzoglou, J. T.; Dobrowski, S. Z.; Parks, S. A.; Hegewisch, K. C. Data

Descriptor: TerraClimate, a high-resolution global dataset of monthly climate and climatic water balance from 1958-2015. *Sci. Data* **2018,** *5*, 1-12.

47. Sacks, W. J.; Deryng, D.; Foley, J. A.; Ramankutty, N. Crop planting dates: an analysis of global patterns. *Glob. Ecol. Biogeogr.* **2010,** *19* (5), 607-620.

48. Wang, H. Y.; Zhang, D.; Zhang, Y. T.; Zhai, L. M.; Yin, B.; Zhou, F.; Geng, Y. C.; Pan, J., T.; Luo, J. F.; Gu, B. J.; Liu, H. B. Ammonia emissions from paddy fields are underestimated in China. *Environ. Pollut.* **2018,** *235*, 482-488.

49. Yang, H.; Zhou, F.; Piao, S. L.; Huang, M. T.; Chen, A. P.; Ciais, P.; Li, Y.; Lian, X.; Peng, S. S.; Zeng, Z. Z. Regional patterns of future runoff changes from Earth system models constrained by observation. *Geophys. Res. Lett.* **2017,** *44* (11), 5540-5549.

50. Wang, Q. H.; Zhou, F.; Shang, Z. Y.; Ciais, P.; Wilfried, W.; Jackson, R. B.; Tubiello, F. N.; Janssens-Maenhout, G.; Tian, H. Q.; Cui, X. Q.; Josep, G. C.; Piao, S. L.; Tao, S. Data-driven estimates of global nitrous oxide emissions from croplands. *National Science Review* **2019,** *7* (2), 441–452.

51. Zhang, B. W.; Tian, H. Q.; Lu, C. Q.; Dangal, S. R. S.; Yang, J.; Pan, S. F. Global manure nitrogen production and application in cropland during 1860-2014: a 5 arcmin gridded global dataset for Earth system modeling. *Earth Syst. Sci. Data* **2017,** *9* (2), 667-678.

52. FAOSTAT. http://www.fao.org/faostat/en/#data/RFN (Fertilizers by Nuntrient); http://www.fao.org/faostat/en/#data/EMN (Livestock Manure); http://www.fao.org/faostat/en/#data/GA (Crop Residues);

http://www.fao.org/faostat/en/#data/GT (Emissions-Agriculture); http://www.fao.org/faostat/en/#data/RL (Tillage fractions); http://www.fao.org/faostat/en/#data/OA (Rural populations and Cropland area).

53. Agricultural Product Cost-Benefit Compilation of China (2001 and 2005). http://tongji.cnki.net/kns55/Navi/NaviSearch.aspx?v=%E5%B9%B4%E9%89%B4%E6%A3%80%E7%B4%A2%E4%B8%AD%E6%96%87%E5%90%8D&n=%E5%85%A8%E5%9B%BD%E5%86%9C%E4%BA%A7%E5%93%81&t=T&IsSubscribe=0&dbstyle=tj.

54. Cao, P. Y.; Lu, C. Q.; Yu, Z. Historical nitrogen fertilizer use in agricultural ecosystems of the contiguous United States during 1850-2015: application rate, timing, and fertilizer types. *Earth Syst. Sci. Data* **2018,** *10* (2), 969-984.

55. Aneja, V. P.; Schlesinger, W. H.; Erisman, J. W.; Behera, S. N.; Sharma, M.; Battye, W. Reactive nitrogen emissions from crop and livestock farming in India. *Atmos. Environ.* **2012,** *47*, 92-103.

56. IFASTAT. https://www.ifastat.org/databases/supply-trade.

57. Femke, L.; Jetse, J. S.; Christoph, M. Options to model the effects of tillage on N_2O emissions at the global scale. *Ecological Modelling* **2019,** *392*, 212–225.

58. China's Agricultural Machinery Industry Yearbook. http://data.cnki.net/Yearbook/Single/N2006090369.

59. Conservation Technology Information Center data. https://www.ctic.org/CRM.

60. EUROSTAT. https://ec.europa.eu/eurostat/statistics-explained/index.php?title=File:Tilled_arable_area_by_tillage_practice,_EU-

27,_IS,_NO,_CH,_ME_and_HR,_2010.png&oldid=137925#file.

61. National Bureau of Statistics of China. http://data.stats.gov.cn/easyquery.htm?cn=C01.

62. Zhang, X.; Davidson, E. A.; Mauzerall, D. L.; Searchinger, T. D.; Dumas, P.; Shen, Y. Managing nitrogen for sustainable development. *Nature* **2015,** *528* (7580), 51-59.

63. Eyring, V.; Lamarque, J.-F.; Hess, P.; Arfeuille, F.; Bowman, K.; Chipperfiel, P. M.; Duncan, B.; Fiore, A.; Gettelman, A.; Giorgetta, A. M.; Granier, C.; Hegglin, M.; Kinnison, D.; Kunze, M.; Langematz, U.; Luo, B. P.; Martin, R.; Matthes, K.; Newman, A. P.; Peter, T.; Robock, A.; Ryerson, T.; Saiz-Lopez, A.; Salawitch, R.; Schultz, M.; Shepherd, G. T.; Shindell, D.; Staehelin, J.; Tegtmeier, S.; Thomason, L.; Tilmes, S.; Vernier, J.-P.; Waugh, W. D.; Young, J. P. Overview of IGAC/SPARC Chemistry-Climate Model Initiative (CCMI) community simulations in support of upcoming ozone and climate assessments. SPARC Newsletter, No. 40, SPARC International Project Office, Oberpfaffenhofen, Germany, 48–66, www.sparc-climate.org/fileadmin/customer/6_Publications/Newsletter_PDF/40SPARCnewsletter_Jan2013_web.pdf. **2013**, 48-66.

64. Bouwman, L.; Goldewijk, K. K.; Van Der Hoek, K. W.; Beusen, A. H. W.; Van Vuuren, D. P.; Willems, J.; Rufino, M. C.; Stehfest, E. Exploring global changes in nitrogen and phosphorus cycles in agriculture induced by livestock production over the 1900-2050 period. *Proc. Natl. Acad. Sci. U. S. A.* **2013,** *110* (52), 20882-20887.

65. Liu, J. G.; You, L. Z.; Amini, M.; Obersteiner, M.; Herrero, M.; Zehnder J. B. A.; Yang, H. A high-resolution assessment on global nitrogen flows in cropland. *Proc. Natl.*

Acad. Sci. U. S. A. **2010,** *107* (17), 8035–8040.

66. Smith, A. P.; Johnson, I. R.; Schwenke, G.; Lam, S. K.; Suter, H. C.; Eckard, R. J. Predicting ammonia volatilization from fertilized pastures used for grazing. *Agricultural and Forest Meteorology* **2020,** *287*, 107952.

67. van Grinsven; Hans, J. M.; Lex, B.; Kenneth, G. C.; Harold. M. van Es; Michelle L. M.; B., A. H. W. Losses of Ammonia and Nitrate from Agriculture and Their Effect on Nitrogen Recovery in the European Union and the United States between 1900 and 2050. *Journal of Environmental Quality* **2015,** *44*, 356-367.

68. Guo, Y. X.; Chen, Y. F.; Searchinger, D. T.; Zhou, M.; Da, P.; Yang, J. N.; Wu, L.; Cui, Z. L.; Zhang, W. F.; Zhang, F. S.; Ma, L.; Sun, Y. L.; Zondlo, A. M.; Zhang, L.; Mauzerall, L. D. Air quality, nitrogen use efficiency and food security in China are improved by cost-effective agricultural nitrogen management. *Nature Food* **2020,** *1*, 648–658.

69. Cui, Z. L.; Zhang, H. Y.; Chen, X. P.; Zhang, C. C.; Ma, W. Q.; Huang, C. D.; Zhang, W. F.; Mi, G. H.; Miao, Y. X.; Li, X. L.; Gao, Q.; Yang, J. C.; Wang, Z. H.; Ye, Y. L.; Guo, S. W.; Lu, J. W.; Huang, J. L.; Lv, S. H.; Sun, Y. X.; Liu, Y. Y.; Peng, X. L.; Ren, J.; Li, S. Q.; Deng, X. P.; Shi, X. J.; Zhang, Q.; Yang, Z. P.; Tang, L.; Wei, C. Z.; Jia, L. L.; Zhang, J. W.; He, M. R.; Tong, Y. N.; Tang, Q. Y.; Zhong, X. H.; Liu, Z. H.; Cao, N.; Kou, C. L.; Ying, H.; Yin, Y. L.; Jiao, X. Q.; Zhang, Q. S.; Fan, M. S.; Jiang, R. F.; Zhang, F. S.; Dou, Z. X. Pursuing sustainable productivity with millions of smallholder farmers. *Nature* **2018,** *555* (7696), 363-366.

70. Zhang, J. L.; Van Der Heijden, G. A. M.; Zhang, F. S.; Bender, S. F. Soil

biodiversity and crop diversification are vital components of healthy soils and agricultural sustainability. *Frontiers of Agricultural Science and Engineering* **2020,** *7* (3), 236–242.

731 **TOC Art**

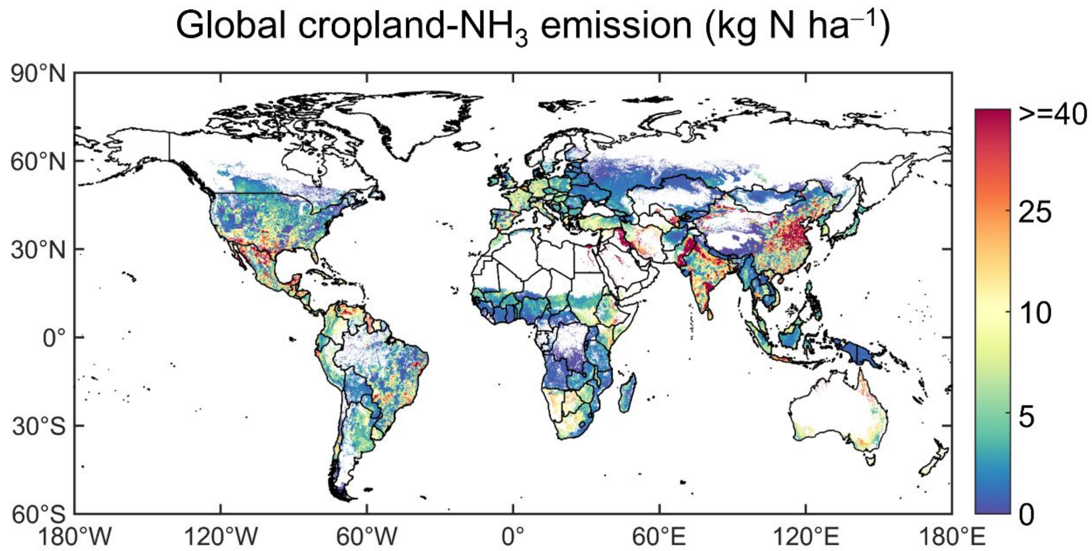

732
733

Figures and tables Captions

Figure 1. Comparison of NH_3 volatilization rate (VR) from our and previous estimates. The numbers in y-axis represent mean value for each bar. For data-driven and process-based methods, dots denote the estimates by individual previous studies (see details in Table S1), and error bars indicate the standard deviation.

Figure 2. Global distribution of cropland-NH_3 volatilization rate (VR; a), NH_3 emissions (V; b) and emission intensity (EI; c) in 2000. The numbers within the panels a and b indicate the values of VR and V for the top ten emitting crops.

Figure 3. Cropland-NH_3 emissions and intensities of the top ten emitting crops mainly providing calorie (a) and countries (b). Values in brackets represent the share of global total emission. Dashed lines denote the global average, twice, and triple intensities.

Figure 4 Cumulative abatement potential of global cropland-NH_3 emissions under different scenarios. S1 represents the scenario where total N input were reduced to achieve the crop-specific NUE targets; S2 represents the scenario where the proportion of ABC and urea was capped at 21.8% and all fertilizers except anhydrous ammonia were incorporated in soils; S1+S2 represents the combination of scenarios 1 and 2. Values in brackets represent the share of cumulative abatement potentials by 20% of global harvested areas for top ten emitting crops.

Figure 5 Global distribution of NH_3 abatement potentials under different scenarios. Left column indicates the quantity of abatement potentials under scenario S1 (a), S2 (c), and S1+S2 (e); Right column indicates the proportion of abatement potentials to the NH_3 emissions under scenario S1 (b), S2 (d), and S1+S2 (f). The definitions of different scenarios can be found in **Figure 4**. Note that the unit of V differs with that in **Figure 2**.

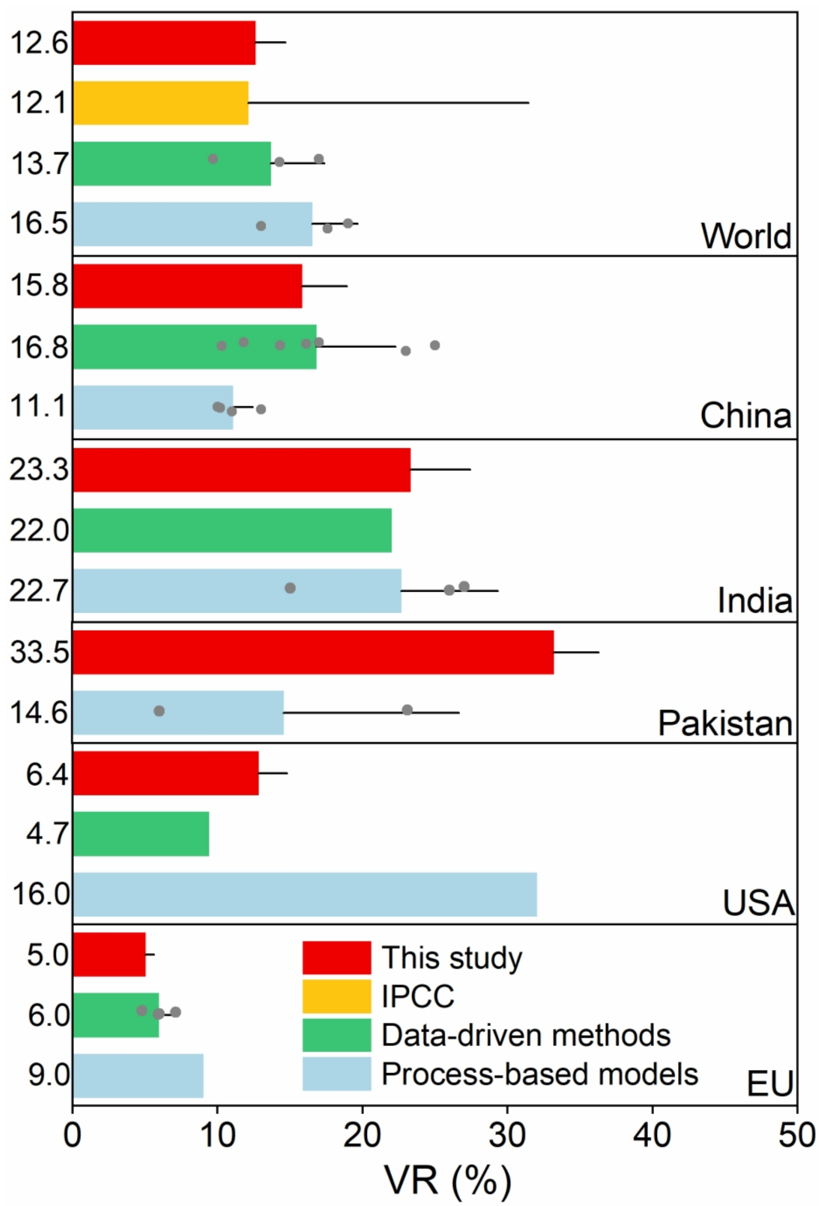

Figure 1. Comparison of NH_3 volatilization rate (VR) from our and previous estimates.

135x198mm (300 x 300 DPI)

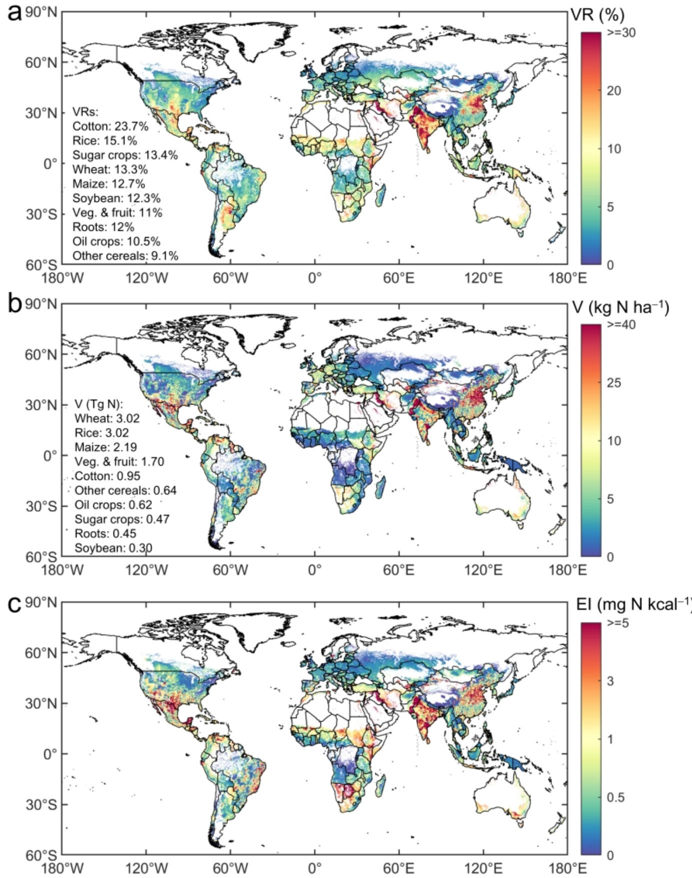

Figure 2. Global distribution of cropland-NH_3 volatilization rate (VR; a), NH_3 emissions (V; b) and emission intensity (EI; c) in 2000.

399x399mm (300 x 300 DPI)

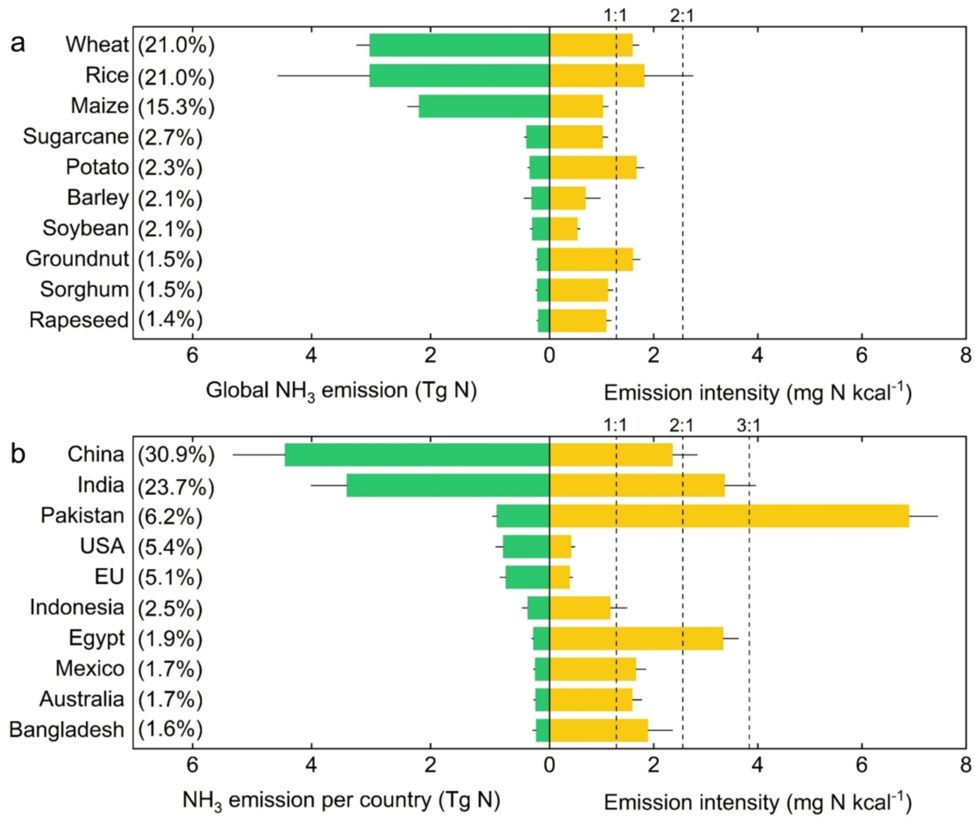

Figure 3. Cropland-NH_3 emissions and intensities of the top ten emitting crops mainly providing calorie (a) and countries (b).

204x170mm (300 x 300 DPI)

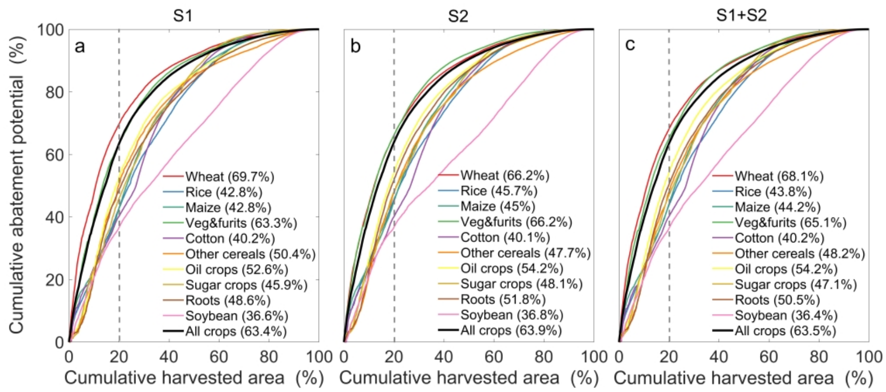

Figure 4 Cumulative abatement potential of global cropland-NH_3 emissions under different scenarios.

503x254mm (300 x 300 DPI)

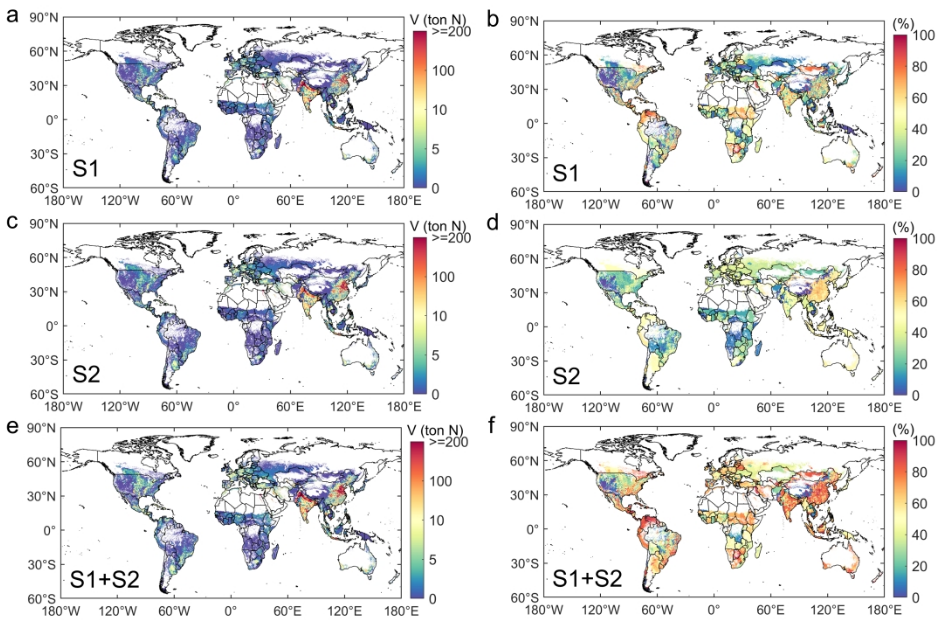

Figure 5 Global distribution of NH_3 abatement potentials under different scenarios.

299x190mm (300 x 300 DPI)